Astron. Astrophys. 318, 256–268 (1997)

ASTRONOMY AND ASTROPHYSICS

Planetary nebulae morphologies, central star masses and nebular properties⋆

S.K. Górny[1,2], **G. Stasińska**[2], **and R.Tylenda**[1]

[1] Copernicus Astronomical Center, Laboratory of Astrophysics, ul. Rabiańska 8, PL-87100 Toruń, Poland (skg@ncac.torun.pl, tylenda@ncac.torun.pl)

[2] DAEC, Observatoire de Meudon, F-92195 Meudon Principal Cedex, France (grazyna@obspm.fr)

Received 2 April 1996 / Accepted 27 June 1996

Abstract. We have constituted a sample of about 80 PN with defined morphologies and well observed basic parameters (fluxes, angular radii, expansion velocities and magnitudes of the central stars). For these PN, we have derived the central star masses by comparing the observed set of parameters with those predicted by a simple evolutionary model of a PN, expanding at the same velocity as the observed one. We have then examined the relations between the PN morphological types and other properties, linked to the central star mass.

Bipolar PN are shown to have a wider distribution of central star masses than the rest of PN, and shifted towards higher values. They lie closer to the Galactic plane and tend to have larger N/O ratios.

Point symmetric PN, which have not been much studied so far, are found to constitute an outstanding class. They show an almost perfect $M_* - v_{\rm exp}$ correlation. They correspond to a rather short evolutionary stage of PN. They lie, on average, further from the Galactic plane than bipolar PN and tend to have lower N/O.

Globally, PN with higher central star masses are found closer to the Galactic plane, and the observed relation between N/O and M_* is roughly consistent with the predictions from evolutionary models for AGB stars.

Key words: planetary nebulae: general – stars: AGB and post-AGB – stars: fundamental parameters

1. Introduction

Planetary nebulae (hereinafter PN) are the "optically visible" manifestation of the late stages of evolution of intermediate mass stars, when the hot stellar remnant ionizes the matter lost at earlier epochs. The mechanism by which these objects are formed is reflected in their morphology. The General Interacting Stellar Winds (GISW) scenario of Balick (1987) can account for many of the observed morphologies (Frank et al. 1993, Frank & Mellema 1994).

For example, in the GISW scheme, bipolar PN are produced by the interaction of a fast, tenuous wind with an equatorially enhanced slow wind. Statistically, bipolar PN tend to have a higher N/O ratio and are found closer to the galactic plane (Peimbert & Torres Peimbert 1983, Corradi & Schwarz 1995), which indicates higher progenitor masses compared to other classes of PN.

The status of point symmetric PN is less clear. The GISW scheme has difficulties in explaining this morphology (Frank & Mellema 1994). It has been suggested (Livio 1994) that point symmetric morphologies may arise from the production of highly collimated outflows by accretion discs formed after the common envelope phase of a binary system.

Recent CCD imaging surveys of PN have motivated new investigations on the correlation between PN morphologies and other properties of the nebulae and their central stars (Stanghellini et al. 1993, Corradi & Schwarz 1995, Amnuel 1995). Obviously, one important issue is whether there exists a relation between the morphology and the central star mass. Stanghellini et al. (1993) found that bipolar nebulae tended to have a flatter central star mass distribution than other morphological classes. Amnuel (1995) found that they had on average more massive central stars. However, the derivation of central star masses is a difficult problem. In Stanghellini et al. (1993) – as in many other studies – the central star masses were simply judged from the comparison of the location of these stars in the HR diagram with stellar evolutionary tracks of different masses. The stellar parameters were derived by the Zanstra method. This induces important biases, as shown by Stasińska & Tylenda (1990). Amnuel (1995) used central star mass estimates adopting a distance scale based on a classification of PN into different mass classes according to a variety of empirical criteria. Other methods for deriving central star masses compare the positions of observed objects with tracks followed by model PN

Send offprint requests to: S.K. Górny

⋆ Table 1 is also available in electronic form and Table 3 is only available in electronic form at the CDS via anonymous ftp 130.79.128.5

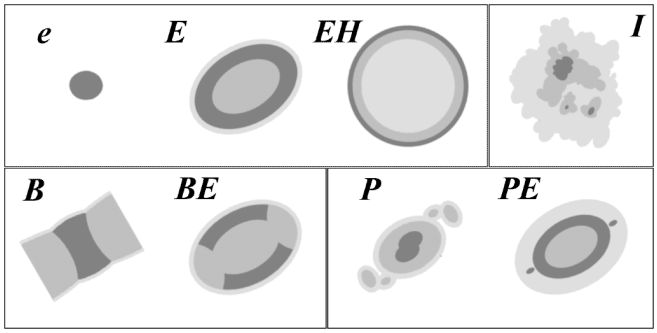

Fig. 1. Sketches of the morphological types adopted for the classification scheme

surrounding stars of various masses. These tracks are obtained from purely theoretical stellar tracks by applying to the model PN the treatment used for observed PN in the derivation of the stellar parameters (Zhang & Kwok 1993, Górny et al. 1993). Such a procedure eliminates the biases mentioned above.

The aim of the present paper is to derive the central star masses for all the PN for which we could assign a morphological class. These masses are derived using an approach similar to Górny et al. (1993), taking due account of the observed nebular expansion velocities in the determination of the theoretical tracks to which the observed PN are to be compared. In Section 2, we describe the observational data base. In Section 3, we present the theoretical evolutionary diagrams that were used for the diagnostics. In Section 4, we examine the positions of the different morphological types of PN in these diagrams. In Section 5, we derive the central star masses for all the PN of our sample, and compare the distributions obtained for different morphological types. In Section 6 we investigate the relation between central star masses and other PN properties within the various morphological classes. The main conclusions are summarized in Section 7.

2. The observational data base

We have considered all the PN from the imaging surveys of Chu et al. (1987), Schwarz et al. (1992) and Bässgen & Bremer (1993), which have been classified by Górny & Stasińska (1995) as *P* (for point symmetric), *B* (for bipolar), *E* (for elliptical) or *I* (for irregular). We have subdivided the point symmetric class into *PE* and *P*, according to whether the knots are embedded or not in an overall elliptical structure. The same procedure was applied for the bipolar nebulae, divided into *BE* and *B*. The elliptical nebulae were subdivided into *e*, which appear like an elliptical disk without structure, *E*, which have a clear elliptical morphology, and *EH* which are almost circular with a very regular shape and a bright rim, suggesting a hollow sphere. Sketches illustrating these criteria are shown in Fig. 1.

This classification scheme was inspired by the one proposed by Stanghellini et al. (1993), the only conceptual difference being the introduction of the *BE*, *PE*, *EH* and *e* subclasses. In a number of cases, the differences in the morphological classes assigned by Stanghellini et al. (1993) and by ourselves result from a different interpretation of a given picture.

The distribution of PN among various morphological classes is not only subjective, but also affected by selection effects, since young *B* (or *P*) nebulae may be sometimes erroneously ascribed an *e* type if they have small angular sizes. In addition, a few of the PN classified as elliptical might actually be bipolar PN seen pole on. This could be the case of NGC 7293 for example, for which additional arguments pointed out by the referee seem to indicate a bipolar nature.

For the diagrams that we consider, we need to know the following parameters: the nebular Hβ flux, the nebular angular diameter, the B or V apparent magnitude of the central star, and the expansion velocity. All these parameters are taken from the compilation presented in Tylenda & Stasińska (1994), who retained only objects for which the data were considered reliable. The reddening correction procedure is the same as in Tylenda & Stasińska (1994).

Central star mass derivations require a consistent set of stellar evolution models for different masses. Therefore, from the present study we have discarded those PN whose central stars are known to be H-poor (Méndez 1991). Indeed, the available stellar model grids are not relevant for this type of objects.

For similar reasons we have also excluded PN with central stars that are known to be binaries. An additional argument is that for most of these objects the observed stellar magnitudes do not refer to the ionizing star but rather to a cooler companion.

Table 1[1] lists the objects considered in our study: i.e. all the PN for which we could assign a morphological class, for which all the relevant data were available and of good quality, and whose central stars are not known to be H-poor or binary. Column 1 gives the PN G name, Column 2 the usual name, and Column 3 the morphological class. The contents of the next columns are described in the following sections.

3. Theoretical evolutionary diagrams to infer central star masses

The evolution of the central star is taken from the grid of H-burning models of Blöcker (1995) for central stars with masses, M_*, of 0.605, 0.625, 0.696, 0.836, 0.940 $M_\odot$, and from Schönberner (1983) for 0.546 and 0.565 $M_\odot$. The definition of the zero-age point in the Schönberner models (epoch when log T_{eff} = 3.7) is not entirely consistent with the one adopted by Blöcker (epoch when radial pulsation period is 50 days), but as explicited in Tylenda & Stasińska (1994), this induces only a minor effect.

As mentioned in the introduction, observations of PN nuclei cannot be directly compared to theoretical evolutionary tracks, because of the biases in the determination of the stellar luminosities and effective temperatures. We have thus adopted an approach similar to the one outlined in Stasińska & Tylenda (1990) and Górny et al. (1993). We have considered a model in which each evolving PN nucleus is surrounded by a sphere of

[1] Table 1 is also available in electronic form at the CDS

nebular matter having a constant density and a filling factor of 0.5. The outer rim of the sphere expands at a constant velocity, $v_{\rm exp}$. The Strömgren radius of the H^+ zone is obtained assuming that the star radiates as a blackbody and that the electron temperature is equal to 10 000 K in the nebula. The Zanstra temperature and luminosity of the theoretical central star are then derived in exactly the same way as in the observed PN. In the same way as for the observed objects, distances to the model PN are computed with the Shklovsky method, taking a shining mass of 0.2 $M_\odot$ (independently of the true shining mass in the nebular model) and a filling factor of 0.5. In such a way, one obtains "apparent" evolutionary tracks for the PN central stars, which can be meaningfully compared to the observations.

A large number of diagnostic diagrams can be built, combining various observational parameters. We have chosen to use three diagrams that display different aspects of the PN evolution. For illustration in this section, we plot only the theoretical evolutionary tracks for central stars of 0.565, 0.605 and 0.645 $M_\odot$ as would be recovered from our evolving model PN. The tracks are marked with symbols, in steps of 5000 years, starting from the formation of the PN. The bold portions of the curves correspond to stages where the nebula is optically thick to the H ionizing radiation. The thin portions correspond to density bounded stages. In Fig. 2a-c, the nebula is assumed to have a total mass $M_{\rm neb}$ = 0.2 $M_\odot$. For each of the three central stars, two different curves are shown corresponding to a nebular expansion velocity of 10 km s^{-1} (dotted curves) and 40 km s^{-1} (full curves).

Fig. 2a shows the variations of $L_{\rm Zan}(H)$ versus $T_{\rm Zan}(H)$, i.e. the HI Zanstra luminosity of the central star, versus the HI Zanstra temperature. Compared to the classical H-R diagram, one sees the effect of the overestimated distance to the nebula when it is optically thick, and of the fact that $T_{\rm Zan}(H)$ underestimates the true stellar temperature when the nebula is density bounded (see Tylenda 1993 for comparison).

A similar diagram using the HeII Zanstra temperature instead of the HI Zanstra temperature would produce less distorted apparent tracks with respect to the original stellar tracks, because nebulae are optically thick to HeII ionizing photons for a longer time. But the HeII line is not observable when the central star has an effective temperature below 70 000 K, which is the case of a large proportion of the objects. Moreover, HeII 4686 may be sometimes affected by the contribution of stellar emission. The present study thus concentrates on results obtained with the HI Zanstra method.

Fig. 2b shows the variations of the models in another classical plane: $M_{\rm v}$ versus log $R_{\rm neb}$, where $M_{\rm v}$ is the absolute visual magnitude of the central star, and $R_{\rm neb}$ is the nebular radius, i.e. the external radius of the ionized part of the nebula. Compared to the theoretical evolutionary tracks, the apparent tracks are shifted to the upper right when the nebula is ionization bounded, due to the overestimation of its distance by the Shklovsky method.

Fig. 2c shows the evolution of the models in the (log $S_{\rm H\beta}$, log $S_{\rm v}$) plane, where $S_{\rm H\beta}$ is the surface brightness of the nebula in Hβ, and $S_{\rm v}$ is defined as $F_{\rm v}/(\pi\theta^2)$, where $F_{\rm v}$ is the stellar flux in the V band and θ is the observable nebular angular radius. Note that $S_{\rm v}$ is closely related to the parameter f introduced in Tylenda & Stasińska (1989) and explored in other studies (e.g. Stasińska & Tylenda 1990, Tylenda et al. 1991, Tylenda & Stasińska 1994). Contrary to the two previous diagrams, the ($S_{\rm H\beta}$, $S_{\rm v}$) diagram has not yet been used in studies of the PN evolution. Its principal advantage is that the parameters plotted on the axes are pure combinations of basic observational

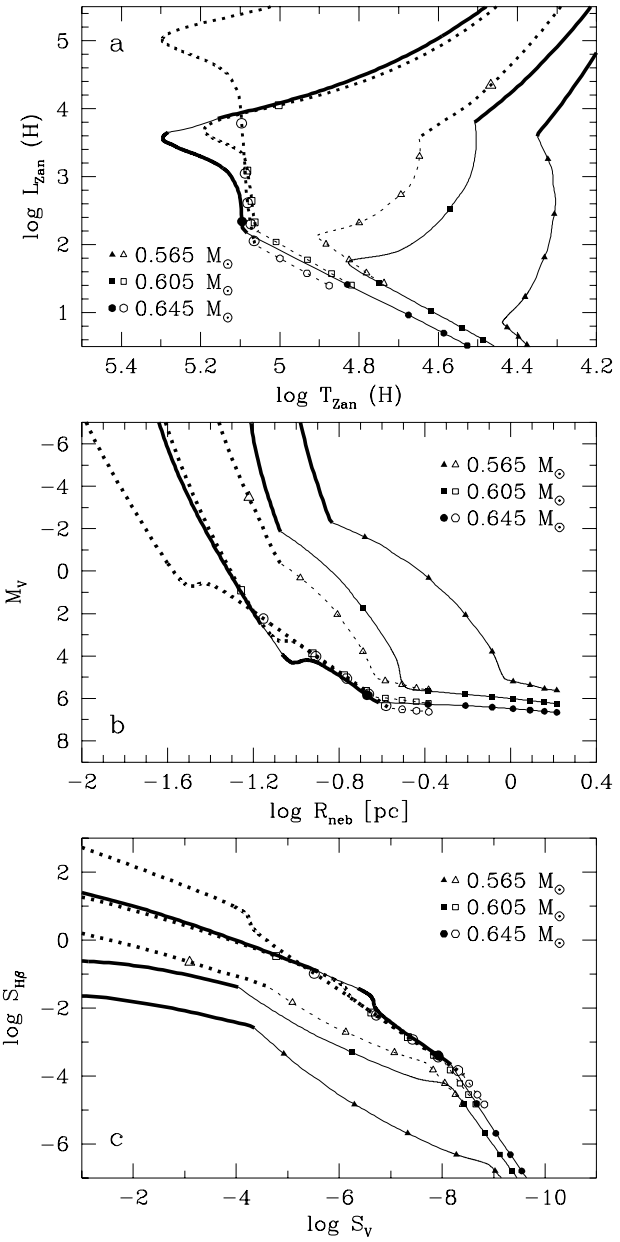

Fig. 2a–c. Apparent evolutionary tracks for stars of masses 0.565, 0.605 and 0.645 $M_\odot$ calculated for a nebular model with $M_{\rm neb}$=0.2$M_\odot$ and different values of the expansion velocity: $v_{\rm exp}$=10 km/s – dotted curves; $v_{\rm exp}$=40 km/s – solid curves. Ionization bounded stages – bold portions; density bounded stages – thin portions. The tracks are marked with symbols every $5 \cdot 10^3$yrs.

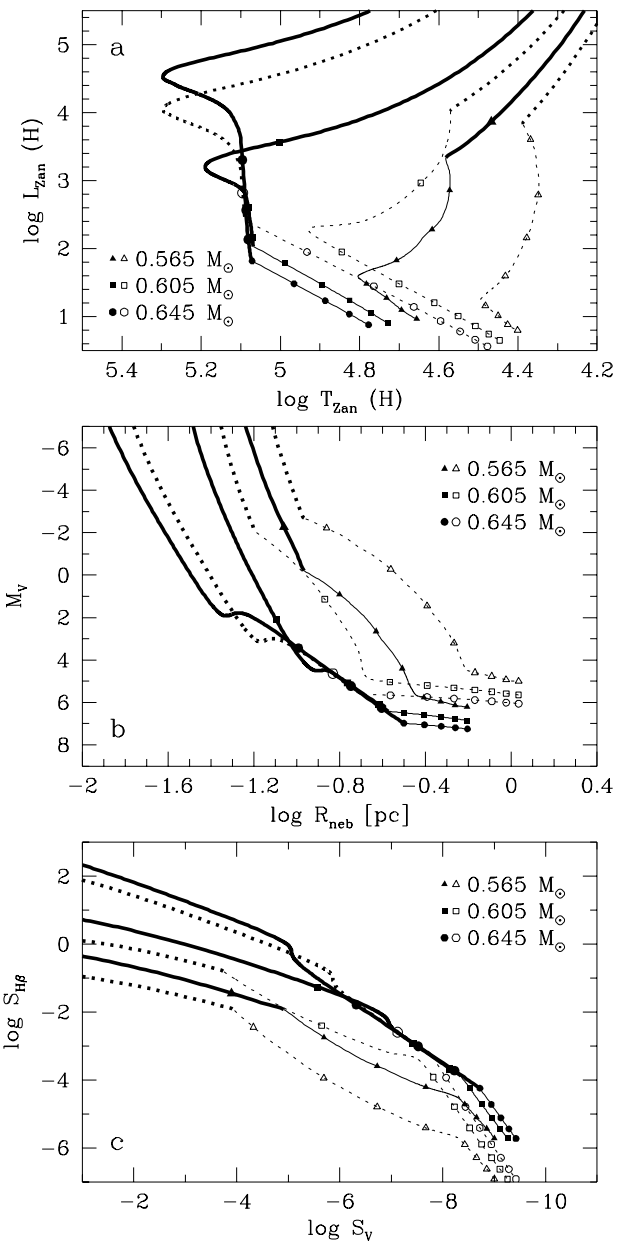

Fig. 3a–c. Apparent evolutionary tracks for stars of masses 0.565, 0.605 and 0.645 $M_\odot$ calculated for a nebular model with v_{exp}=20 km/s and different values of the nebular mass: M_{neb} =0.1$M_\odot$ – dotted curves; M_{neb} =0.4$M_\odot$ – solid curves. Ionization bounded stages – bold portions; density bounded stages - thin portions. The tracks are marked with symbols every $5 \cdot 10^3$yrs.

data and do not involve any assumption. Thus the positions of the observed objects in this diagram are well defined and their uncertainties are determined only by the precision of the observations. In the two previous diagrams the observed positions may change significantly depending on assumptions and methods used to derive the stellar temperature and/or the distance. The parameters plotted in this diagram have an important meaning from the point of view of the PN evolution. $S_{H\beta}$ is a sort of measure of the expansion stage of the nebula. S_v plays a similar role for the evolutionary stage of the central star. S_v is a mean surface brightness which the nebula would have in the V band if it were a purely scattering nebula. Thus the ($S_{H\beta}$, S_v) diagram can be used for investigating the evolutionary state of the central star with respect to the expansion state of the nebula.

The positions of the theoretical tracks in our diagrams depend not only on the central star mass but also on the principal parameters of the model nebula, i.e. its mass and expansion velocity. As can be seen from Fig. 2a-c the effect of the expansion velocity on the apparent tracks is important. For example, a central star of M_* = 0.60 $M_\odot$ with a nebula expanding at v_{exp} = 40 km s^{-1} mimics a star of M_* = 0.56 $M_\odot$ with a nebula expanding at v_{exp} = 10 km s^{-1}.

The reason why the apparent tracks depend on v_{exp} is that this parameter fixes the deviation from the case where the assumptions for the Zanstra method or for the Shklovsky method are correct. At a given time, the ionizable mass is proportional to the cube of the expansion velocity. Therefore a larger expansion velocity results in a smaller error on the Shklovsky distance at any time when the nebula is still optically thick. In addition, the optically thin regime, when the Shklovsky distances are correct, is reached sooner, at a time where the star is cooler. When it is reached, the error on the star temperature derived by the Zanstra method depends on the ratio of the mass of the nebula and of the mass that could be ionized by the star at that time. When v_{exp} is larger, the underestimation of the star temperature by the Zanstra method is therefore more important. For all these reasons, the apparent track of a star of given mass in the ($L_{Zan}(H)$, $T_{Zan}(H)$) diagram resembles that of a star of larger mass surrounded by a nebula of larger expansion velocity. Similar effects are observed on the two other diagrams.

The effect of the nebular mass on the theoretical tracks in the diagrams can be seen from Fig. 3a-c, which is the counterpart of Fig. 2a-c but for v_{exp} = 20 km s^{-1} with M_{neb} = 0.1 $M_\odot$ (dotted line) and 0.4 $M_\odot$ (solid line). Comparing Fig. 3 with Fig. 2 one finds that the factor 4 in M_{neb} has less important effects on the apparent tracks than the same factor in v_{exp}. M_{neb} especially affects those parts of the tracks which correspond to the nebula being completely ionized. Higher M_{neb} means then higher Hβ luminosity which correspondingly affects the parameters plotted in our diagrams. If the model nebula is partly ionized the Hβ luminosity reflects the ionizing flux of the central star and the exact value of M_{neb} is not important. In our model however, M_{neb} determines the nebular density and thus the size of the ionized part of the nebula in the radiation bounded phase. This has its influence on the Shklovsky distance as well as on the values of $S_{H\beta}$ and S_v.

4. Distribution of the PN morphological classes in the diagnostic diagrams

Columns 4 through 10 of Table 1 list the values of log $T_{Zan}(H)$, log $L_{Zan}(H)$ (in solar units), M_v, log R_{neb} (in pc), log S_v (in erg cm^{-2} sec^{-1} sr^{-2}), log $S_{H\beta}$ (in erg cm^{-2} sec^{-1} sr^{-2}) and of the Shklovsky distance (in kpc) for the observed PN.

Table 1. Planetary nebulae properties and derived central stars masses, evolutionary ages and distances

PN G	Main Name	type	log $T_{\rm Zan}(H)$	log $L_{\rm Zan}(H)$	$M_{\rm v}$	log $R_{\rm neb}$	log $S_{\rm v}$	log $S_{\rm H\beta}$	$d_{\rm Shk}$	M_*	$t_{\rm ev}$	d
000.3+ 12.2	IC 4634	P	4.63	3.69	-0.81	-1.11	-4.39	-1.22	5.9	0.577	5.3	5.8
002.7−04.8	M 1-42	BE :	4.83	2.96	2.40	-0.90	-6.08	-2.24	5.7	0.567	15.1	5.7
003.5−04.6	NGC 6565	E	5.15	3.14	4.23	-0.93	-6.76	-2.11	5.3	0.609 (0.685)	6.3	5.0
008.0+ 03.9	NGC 6445	B	5.29	3.00	5.58	-0.85	-7.46	-2.50	1.7	0.852	3.4	1.1
009.4−05.0	NGC 6629	E	4.54	3.53	-0.97	-1.00	-4.53	-1.72	2.6	0.561	15.8	2.5
009.6+ 14.8	NGC 6309	P	4.82	3.01	2.22	-0.92	-5.98	-2.15	3.1	0.615	3.8	3.1
010.8+ 18.0	M 2- 9	B	4.62	2.82	1.30	-0.81	-5.83	-2.71	3.7	0.603	4.9	3.7
011.7−00.6	NGC 6567	E :	4.67	3.62	-0.33	-1.10	-4.60	-1.26	4.4	0.603	3.5	4.4
017.6−10.2	A 51	EH	4.54	1.75	3.48	-0.41	-7.50	-4.71	2.4	0.593	9.1	2.4
025.3+ 40.8	IC 4593	E	4.45	3.59	-1.71	-0.95	-4.35	-2.01	3.6	0.561	9.8	3.4
025.8−17.9	NGC 6818	E	5.20	3.21	4.46	-0.94	-6.84	-2.06	2.4	0.621 (0.728)	3.9	2.1
033.1−06.3	NGC 6772	E	5.03	2.21	5.67	-0.64	-7.91	-3.54	1.4	0.601	13.7	1.4
034.5−06.7	NGC 6778	B :	4.91	2.94	3.01	-0.89	-6.34	-2.28	3.4	0.607	5.7	3.4
036.1−57.1	NGC 7293	E :	5.07	1.63	7.42	-0.44	-9.02	-4.55	0.2	0.930	22.2	0.2
037.7−34.5	NGC 7009	P	4.80	3.21	1.61	-0.99	-5.60	-1.82	1.5	0.605	5.0	1.5
041.8−02.9	NGC 6781	E	4.92	2.29	4.71	-0.68	-7.46	-3.36	0.8	0.573	16.9	0.8
043.1+ 03.8	M 1-65	E	4.45	3.81	-2.22	-1.03	-3.98	-1.61	9.7	0.561	10.7	7.3
043.1+ 37.7	NGC 6210	I	4.69	3.40	0.35	-1.03	-5.01	-1.60	2.8	0.605	3.7	2.8
043.3+ 11.6	M 3-27	e	4.57	4.39	-2.94	-1.31	-3.14	-0.22	20.4	0.595	3.0	10.0
045.7−04.5	NGC 6804	BE	4.58	2.78	1.18	-0.78	-5.84	-2.85	2.0	0.593	6.2	2.0
046.4−04.1	NGC 6803	E :	4.69	3.65	-0.25	-1.11	-4.60	-1.18	6.4	0.591	4.6	6.4
054.1−12.1	NGC 6891	PE :	4.54	3.39	-0.63	-0.95	-4.77	-1.98	3.1	0.562	11.9	3.1
062.4+ 09.5	NGC 6765	I	4.58	2.15	2.77	-0.57	-6.89	-3.90	2.8	0.597	7.5	2.8
063.1+ 13.9	NGC 6720	E	5.07	2.58	5.10	-0.76	-7.46	-2.97	1.0	0.611	6.0	0.9
064.6+ 48.2	NGC 6058	E	4.43	2.66	0.51	-0.62	-5.89	-3.66	4.3	0.573	8.6	4.3
065.9+ 00.5	NGC 6842	E	4.64	2.28	2.81	-0.64	-6.77	-3.54	1.7	0.603	6.4	1.7
066.7−28.2	NGC 7094	EH	4.42	2.07	1.90	-0.41	-6.87	-4.70	1.7	0.583	8.8	1.7
083.5+ 12.7	NGC 6826	PE	4.50	3.48	-1.07	-0.96	-4.58	-1.95	1.8	0.565	6.6	1.8
084.9−03.4	NGC 7027	I	5.30	4.38	2.27	-1.30	-5.23	-0.23	1.6	0.652 (0.838)	1.8	0.7
093.4+ 05.4	NGC 7008	E :	4.57	2.43	1.97	-0.66	-6.40	-3.46	1.1	0.603	5.7	1.1
103.2+ 00.6	M 2-51	E	5.20	2.41	6.43	-0.67	-8.15	-3.38	2.1	0.792	18.2	1.9
104.1+ 07.9	NGC 7139	BE :	4.96	1.81	6.21	-0.52	-8.38	-4.17	1.6	0.633	14.7	1.6
114.0−04.6	A 82	B	4.53	1.96	2.88	-0.47	-7.14	-4.39	1.5	0.577	11.8	1.5
122.1−04.9	A 2	E	4.94	1.66	6.43	-0.47	-8.57	-4.42	3.9	0.668	9.8	3.9
123.6+ 34.5	IC 3568	E	4.59	3.33	-0.16	-0.97	-4.93	-1.92	4.5	0.563	13.1	4.5
148.4+ 57.0	NGC 3587	E	5.04	1.86	6.68	-0.52	-8.56	-4.15	0.7	0.854	9.2	0.7
166.1+ 10.4	IC 2149	I :	4.49	3.91	-2.24	-1.09	-3.85	-1.28	4.2	0.577	3.7	3.3
190.3−17.7	J 320	P	4.55	3.28	-0.30	-0.93	-4.95	-2.11	7.0	0.575	6.3	7.0
194.2+ 02.5	J 900	BE	5.01	3.51	2.32	-1.08	-5.70	-1.36	5.8	0.615	3.9	5.8
196.6−10.9	NGC 2022	PE	4.78	2.78	2.52	-0.84	-6.25	-2.55	3.1	0.607	5.4	3.1
197.8+ 17.3	NGC 2392	E	4.43	3.61	-1.82	-0.94	-4.31	-2.03	2.4	0.607	1.9	2.4
206.4−40.5	NGC 1535	E	4.56	3.20	-0.01	-0.91	-5.11	-2.21	2.4	0.581	5.9	2.4
215.2−24.2	IC 418	E	4.57	4.07	-2.08	-1.20	-3.69	-0.73	2.2	0.573	5.1	1.4
221.3−12.3	IC 2165	BE :	5.20	3.56	3.57	-1.05	-6.25	-1.47	4.0	0.617 (0.726)	4.2	3.8
234.8+ 02.4	NGC 2440	B	5.33	3.49	4.70	-1.00	-6.81	-1.75	2.4	0.932	3.4	0.8
239.6+ 13.9	NGC 2610	E	4.70	2.19	3.44	-0.63	-7.05	-3.61	2.6	0.589	9.6	2.6
261.0+ 32.0	NGC 3242	PE	4.74	3.31	0.93	-1.01	-5.28	-1.69	1.6	0.603	4.5	1.6
261.9+ 08.5	NGC 2818	B	5.29	2.27	7.42	-0.60	-8.69	-3.73	2.1	$>$0.940	-	-
264.4−12.7	He 2- 5	e	4.60	3.73	-1.04	-1.10	-4.30	-1.22	10.8	0.565	7.3	9.3
265.7+ 04.1	NGC 2792	E	4.88	3.09	2.46	-0.95	-6.02	-2.01	3.6	0.606	5.5	3.6
285.7−14.9	IC 2448	E :	4.66	3.26	0.48	-0.97	-5.18	-1.89	4.9	0.579	7.3	4.9
286.3−04.8	NGC 3211	E	5.14	2.94	4.67	-0.86	-7.07	-2.44	3.5	0.617 (0.674)	4.5	3.3
292.4+ 04.1	PB 8	E	4.48	3.67	-1.70	-1.00	-4.24	-1.74	8.2	0.561	11.7	7.1
294.1+ 43.6	NGC 4361	E :	4.63	2.45	2.35	-0.69	-6.48	-3.28	1.3	0.597	6.8	1.3
294.6+ 04.7	NGC 3918	P	5.18	3.51	3.53	-1.04	-6.25	-1.52	2.0	0.621 (0.702)	3.6	1.9
298.3−04.8	NGC 4071	E :	5.09	1.98	6.73	-0.55	-8.52	-3.99	1.8	0.698 (0.839)	15.9	1.8
312.3+ 10.5	NGC 5307	P	4.63	3.16	0.56	-0.93	-5.30	-2.11	3.9	0.567	10.3	3.9
315.1−13.0	He 2-131	e	4.52	4.17	-2.69	-1.20	-3.45	-0.74	4.3	0.573	4.6	2.4
316.1+ 08.4	He 2-108	E	4.41	3.53	-1.75	-0.89	-4.45	-2.29	4.8	0.557	20.4	4.5
319.6+ 15.7	IC 4406	B	5.18	2.78	5.37	-0.80	-7.48	-2.75	1.9	0.756	13.8	1.0
326.7+ 42.2	IC 972	E	4.76	1.62	5.31	-0.45	-8.15	-4.50	3.5	0.572	21.5	3.5
327.8+ 10.0	NGC 5882	P	4.71	3.41	0.47	-1.04	-5.04	-1.55	2.7	0.603	4.2	2.7
334.3−09.3	IC 4642	BE	4.75	2.77	2.38	-0.83	-6.21	-2.59	3.7	0.597	6.8	3.7
338.1−08.3	NGC 6326	I	4.92	2.99	2.99	-0.91	-6.30	-2.19	4.1	0.601	7.0	4.1
341.6+ 13.7	NGC 6026	I :	4.41	2.67	0.38	-0.61	-5.87	-3.71	2.6	0.567	9.5	2.6
341.8+ 05.4	NGC 6153	E	4.88	3.28	1.96	-1.01	-5.69	-1.70	1.7	0.603	5.5	1.7
342.1+ 10.8	NGC 6072	B	5.27	2.61	6.44	-0.72	-8.06	-3.14	1.3	0.910	17.4	0.9
342.1+ 27.5	Me 2-1	e	5.17	3.13	4.44	-0.92	-6.86	-2.15	7.1	0.724	7.6	2.6
345.2−08.8	Tc 1	E	4.45	3.82	-2.24	-1.03	-3.98	-1.61	4.1	0.561	8.6	3.1
345.4+ 00.1	IC 4637	E :	4.45	3.65	-1.85	-0.97	-4.25	-1.89	2.4	0.565	4.8	2.2
346.2−08.2	IC 4663	E :	4.62	2.98	0.93	-0.86	-5.57	-2.43	4.3	0.575	8.8	4.3
349.3−01.1	NGC 6337	E	4.62	2.49	2.16	-0.70	-6.39	-3.24	1.6	0.563	24.2	1.6
350.9+ 04.4	H 2- 1	e	4.45	4.33	-3.50	-1.20	-3.13	-0.75	10.4	0.571	4.1	4.8
356.5−02.3	M 1-27	e	4.43	3.87	-2.52	-1.02	-3.88	-1.66	5.7	0.561	10.8	4.0
358.5−07.3	NGC 6563	E :	5.08	2.40	5.59	-0.69	-7.77	-3.27	1.8	0.648	16.6	1.2
358.9−00.7	M 1-26	e	4.48	4.59	-3.96	-1.31	-2.71	-0.17	6.2	0.571	4.3	2.1

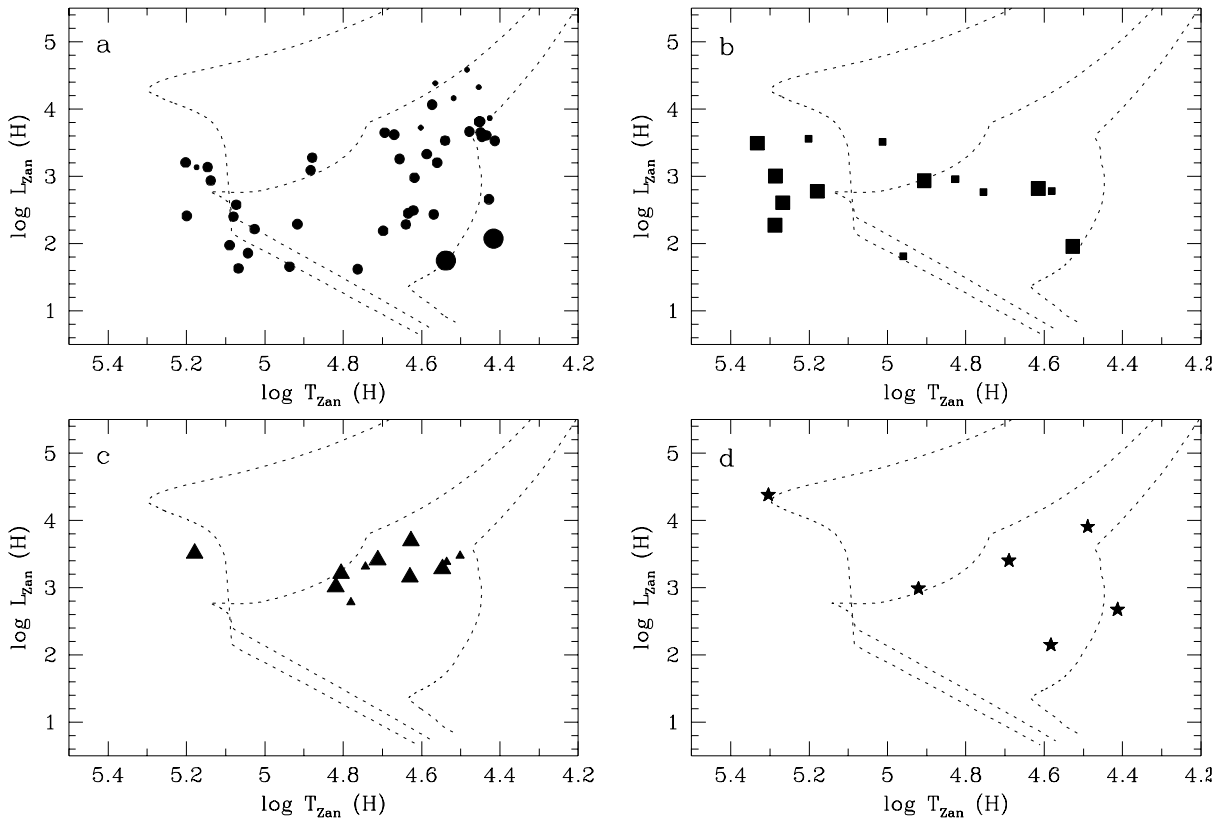

Fig. 4a–d. Distribution of the PN in the HR diagram, according to their morphological class: **a** elliptical: *e* – small circles, *E* – medium circles, *EH* – large circles; **b** bipolar: *B* – large squares, *BE* – small squares; **c** point symmetric: *P* – large triangles, *PE* – small triangles; **d** irregular.

Figs. 4, 5, 6 give the distribution of the PN in the ($L_{\rm Zan}(H)$, $T_{\rm Zan}(H)$) , ($M_{\rm v}$, $R_{\rm neb}$) and ($S_{\rm H\beta}$, $S_{\rm v}$) planes, respectively. The different panels correspond to PN of various morphological classes. Elliptical PN are plotted in Figs. 4 – 6 a. Small circles represent type *e*, medium size circles represent type *E*, and large ones type *EH*. Similarly, bipolar PN are plotted in Figs. 4 – 6 b. Large squares represent type *B* (those which correspond to the definition of Stanghellini et al. 1993), and small squares represent our type *BE*. Point symmetric PN are plotted in Figs. 4 – 6 c, with large symbols for type *P* and small ones for type *PE*. Irregular nebulae are plotted in Figs. 4 – 6 d.

On these diagrams are superimposed, just for reference, the apparent evolutionary tracks for central stars of masses 0.565, 0.605 and 0.645 $M_\odot$, surrounded by a model nebula of mass 0.2 $M_\odot$ and expansion velocity 20 km s^{-1}.

From a glance at Fig. 4 (as well as at Figs. 5 and 6), one might conclude that, for all the morphological types, the central star masses are distributed between roughly 0.64 and 0.56 $M_\odot$, with a peak around 0.58 $M_\odot$, with bipolar PN showing a larger proportion of high mass nuclei.

Strikingly, the point symmetric PN lie in a very restricted zone in each diagram. This is particularly well seen in Fig. 6 where all these objects are observed in a narrow range of $S_{\rm H\beta}$, i.e. log $S_{\rm H\beta} = -1.88 \pm 0.37$ (mean value and standard deviation). One might thus be tempted to conclude that point symmetric nebulae represent only a short evolutionary stage. And, since there appears a well defined limit between the location of the point symmetric PN and the bipolar ones (especially prominent in Fig. 6 at log $S_{\rm v}$= -6.0) one could argue that point symmetric PN represent an early stage of bipolar PN. But, as outlined in the previous section, a proper interpretation of observational data on PN requires a more refined analysis.

Stanghellini et al. (1993) found that all the irregular PN were grouped in the same region of the HR diagram, from which she concluded that their central star masses should be similar. Such a behaviour is not seen in our Fig. 4. This is partly because we considered only HI-Zanstra temperatures and Shklovsky distances, while Stanghellini et al. used HeII-Zanstra temperatures as well and a different distance scale. But this is also due to discrepancies in morphology classification of individual objects between Stanghellini et al. and ourselves, and to the fact that the investigated samples are not the same.

5. Derivation of the central star masses

As discussed in Section 3 the positions of the model tracks in our diagrams depend on the parameters of the adopted model nebula, i.e $M_{\rm neb}$ and $v_{\rm exp}$. Especially the value of $v_{\rm exp}$ is crucial, as can be seen from Fig. 2. Thus, in order to get a reliable estimate

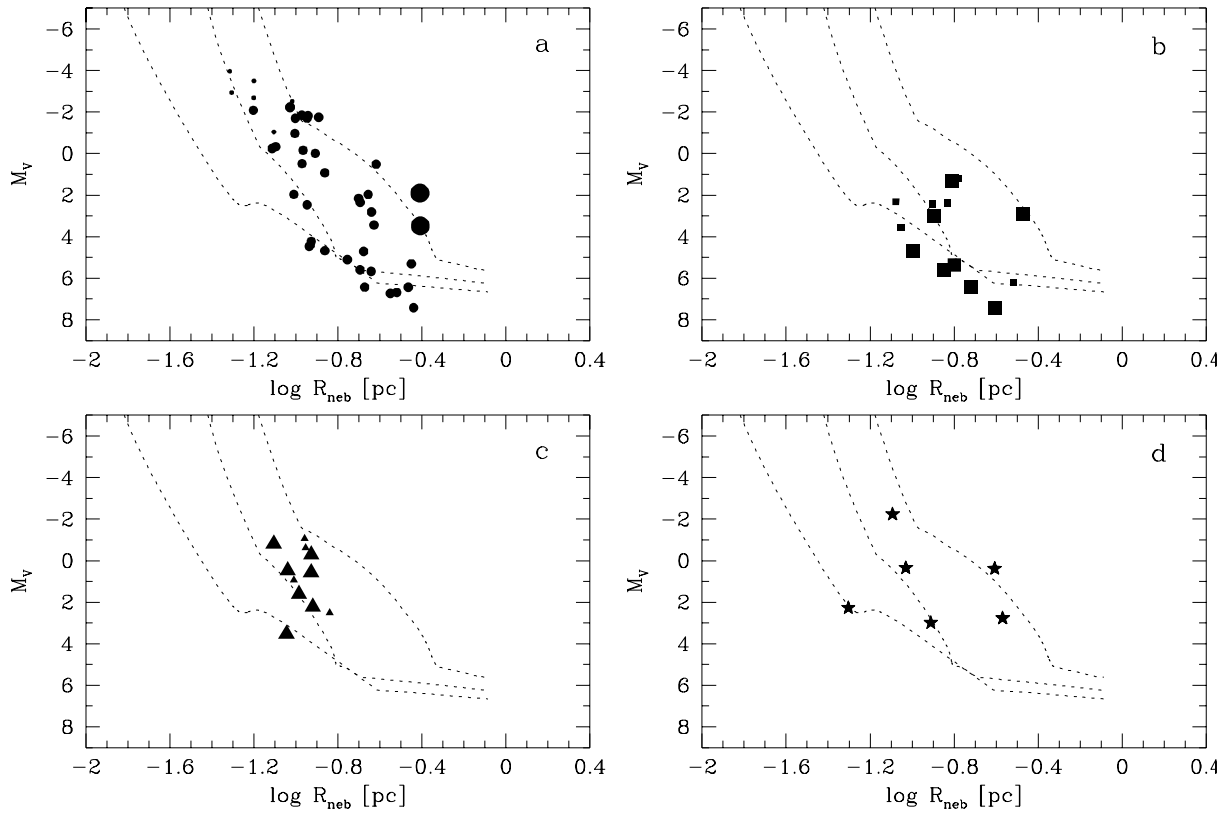

Fig. 5a–d. Distribution of the PN in the $M_{\rm v}$ vs. $R_{\rm neb}$ plane according to their morphological class: **a** elliptical; **b** bipolar; **c** point symmetric; **d** irregular. Same meaning of symbols as in Fig. 4.

of the central star mass from the observed positions of a PN in such diagrams, one needs to know the expansion velocity.[2]

Due to the lack of a reliable method for determining PN distances we cannot estimate $M_{\rm neb}$ for the observed objects. Therefore one has to adopt a value for $M_{\rm neb}$ while deriving central star masses and this is the only free parameter in the framework of our model. Fortunately, in most cases the results are not very sensitive to the value of $M_{\rm neb}$, as discussed below.

In the present study the PN central star masses are derived from comparison of the observed positions to a grid of apparent theoretical evolutionary tracks. The grid of evolutionary tracks for model central stars ranges from 0.54 to 0.94 $M_\odot$ by steps of 0.002 $M_\odot$. It has been obtained by interpolation from the tracks of Blöcker (1995) and Schönberner (1983). The model nebula, used to obtain the apparent tracks has the same mass of 0.2 $M_\odot$ in all cases. However, its expansion velocity is different in each case and is equal to the value observed for a given object. Thus for each observed PN we construct a separate grid of apparent tracks in order to derive its central star mass.

It turns out that the above procedure for the central star mass determination effectively reduces the three diagrams discussed in the previous sections to one only. The reason is that the analysis on any of the three diagrams always requires all the four observational data, i.e. central star magnitude, nebular Hβ flux, nebular angular diameter and nebular expansion velocity. The first three values allow to place the observed object in a diagram. The last one ($v_{\rm exp}$) is used as a parameter of the theoretical tracks. As a result, if an apparent theoretical track passes through the position of a given observed object on one diagram then it means that this model satisfies the set of the observed parameters for this object. Thus it passes necessarily through the observed position of the same object on another diagram which is just another combination of the same parameters.

The central star masses obtained with our procedure and assuming $M_{\rm neb}$ = 0.2 $M_\odot$ are listed in column 11 of Table 1. We have verified that, in our sample, for most of the objects the uncertainties in the observational parameters induce an error of $\pm$0.01 $M_\odot$ at most in the derived central star masses. However, for some of them, corresponding to massive central stars on their cooling tracks, the errors may be much larger. A few objects have a position in the diagrams where several apparent tracks cross each other, leading to an ambiguous mass derivation. Then

[2] Zhang & Kwok (1993) used an approach similar to ours to estimate the masses of PN nuclei. They built apparent tracks for PN whose mass and expansion velocity are given by the two-wind interacting model in the momentum-conserving case. The parameters they chose for the two winds univoquely defined the nebular expansion velocity at a given time. In their models, $v_{\rm exp}$ evolves between 10 and 12 km s^{-1} for a central star of 0.565 $M_\odot$ and 0.598 $M_\odot$, and between 10 and 14 km s^{-1} for a star of 0.644 $M_\odot$. Such values are far from spanning the range of observed values in planetary nebulae

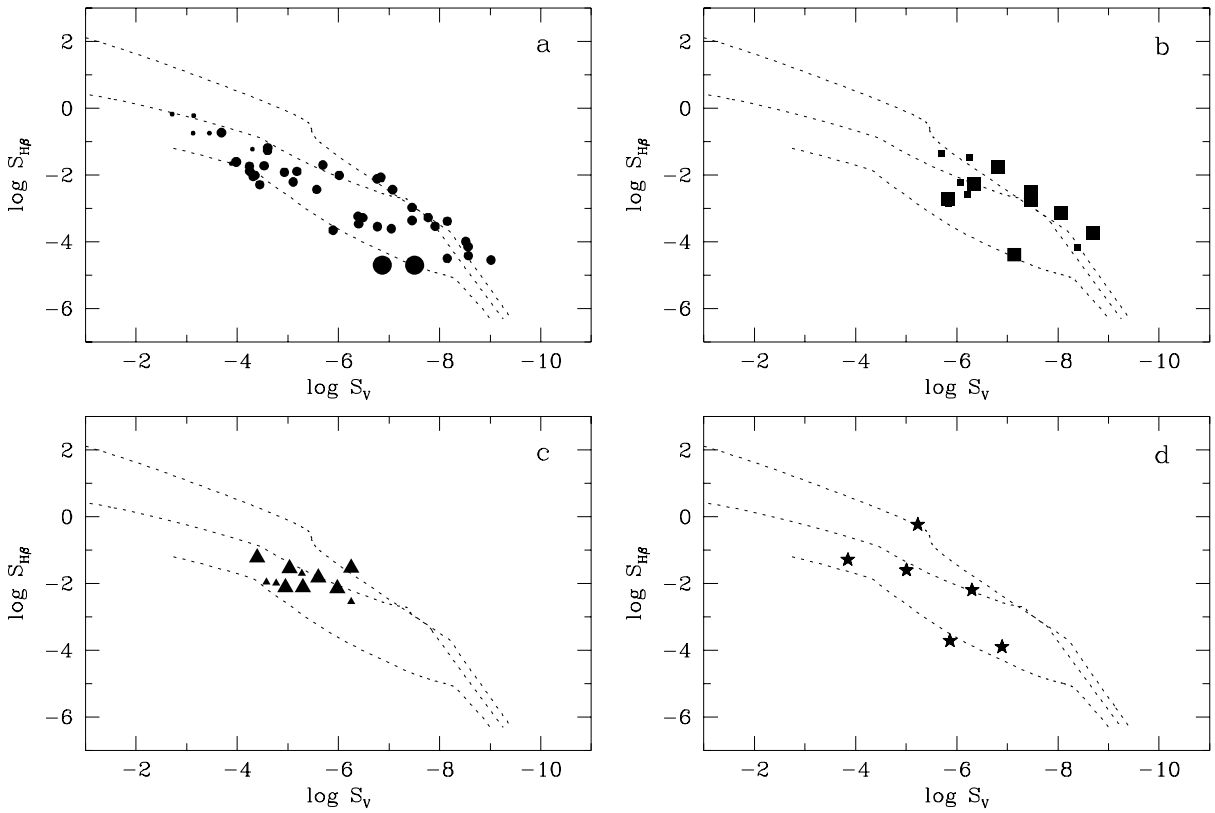

Fig. 6a–d. Distribution of the PN in the $S_{H\beta}$ vs. S_v plane, according to their morphological class: **a** elliptical; **b** bipolar; **c** point symmetric; **d** irregular. Same meaning of symbols as in Fig. 4.

the value given in column 11 corresponds to the lower central star mass compatible with the observation (usually the most probable considering evolutionary timescales), and the upper limit is given in parenthesis.

The influence of the adopted $M_{\rm neb}$ on the derived central star masses is illustrated in Fig. 7. The objects are represented by the same shape of symbols as in Figs. 4-6, with the ordinate corresponding to the value of the central star mass derived using $M_{\rm neb}$ = 0.2 $M_\odot$. The top of the bar corresponds to the derivation taking $M_{\rm neb}$ = 0.1 $M_\odot$ and the bottom to one taking $M_{\rm neb}$ = 0.4 $M_\odot$. Fig. 7 shows that, for stars with masses less than 0.65 $M_\odot$, a range of a factor two in the nebular masses (as seen in the density bounded PN observed in the Magellanic Clouds, Barlow 1987) translates into an uncertainty of only about 0.01 $M_\odot$ in most cases. As seen from Fig. 7, if the typical nebular mass were for example 0.1 $M_\odot$ rather than 0.2 $M_\odot$, the central star masses would be systematically higher by about 0.01 $M_\odot$. At the high star mass end, on the other hand, not knowing $M_{\rm neb}$ may have drastic effects on the derived central star masses. Actually, the magnitude of the uncertainty for a given object depends on its location in the diagrams. For example, most of the bipolar PN happen to lie in a place where the uncertainty on the central star mass is small, as seen in Fig. 7. On the other hand, the uncertainty for some of the elliptical PN is very large.

From now on, M_* will refer to the central star masses appearing in Table 1.

Instead of adopting a nebular model with a constant $M_{\rm neb}$ and a constant $v_{\rm exp}$, we could have adopted a model in which the expansion velocity evolves with time, and in which the nebula gradually sweeps up material from the slow ABG wind, as in the model of Zhang & Kwok (1993). At present it is however unknown what parameters should be adopted for such a model to get the best approximation for the entire PN population, making the results similarly model-dependent with more free parameters than in the case of our simple nebular model (see footnote 2).

6. The relation between central star masses, PN morphologies and other properties

6.1. The M_* distribution for different morphological types

Table 2 compares, for the different morphological types, the mean and standard deviation of the M_* distribution. The number of PN with derived M_* in each class is given in parenthesis. This table indicates that the bipolar PN have, on average, higher central star masses than the rest of PN in our sample. This is confirmed by the Mann-Whitney test at the 99% confidence level. In particular, bipolar PN tend to have higher central star masses than elliptical PN or point symmetric ones (however,

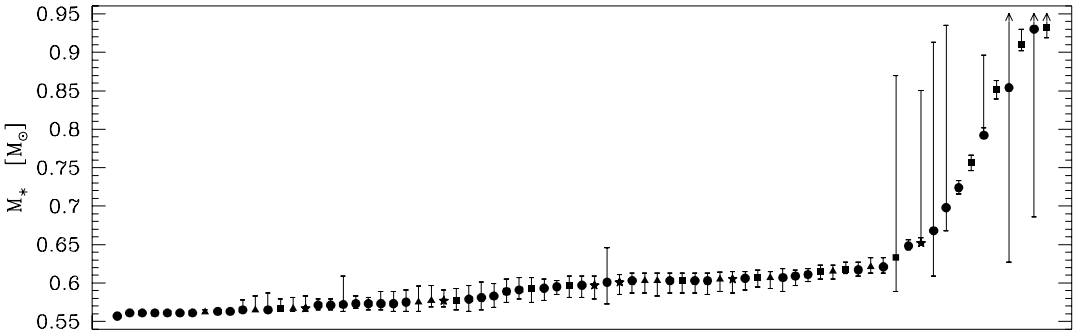

Fig. 7. Central star masses for the sample of PN with known expansion velocities, derived assuming different nebular masses. The objects are ordered according to the value of M_*, obtained adopting M_{neb}=0.2$M_\odot$, and represented by a symbol whose ordinate is equal to M_*. The top of the bar corresponds to the derivation taking $M_{\rm neb}$ = 0.1 $M_\odot$, the bottom taking $M_{\rm neb}$ = 0.4 $M_\odot$. Meaning of symbols: circles – elliptical (*e*, *E* & *EH*); squares – bipolar (*B* & *BE*); triangles – point symmetric (*P* & *PE*); stars – irregular (*I*).

Table 2. Statistics of PN according to their morphological types

	M_* [$M_\odot$]			|z| [kpc]			log N/O		
	mean	σ	nb	mean	σ	nb	mean	σ	nb
elliptical	0.610	0.077	(45)	0.68	0.77	(45)	-0.56	0.33	(57)
bipolar	0.681	0.133	(13)	0.36	0.32	(13)	-0.25	0.46	(15)
pointsymmetric	0.591	0.022	(11)	0.80	0.52	(11)	-0.78	0.38	(16)
irregular	0.600	0.030	(6)	0.67	0.56	(6)	-0.36	0.25	(10)

the statistics is rather poor in the latter case). Note also, from Table 1, that one third of the bipolar PN have $M_*>$ 0.7 $M_\odot$, all these objects being of *B* and not *BE* type. There is no evidence of a segregation in central star mass between elliptical, point symmetric and irregular PN.

6.2. The M_* – $v_{\rm exp}$ relation

Fig. 8 shows the nebular expansion velocity as a function of M_*, with the same meaning of the symbols as in Fig. 4 (except that all the PN are now represented in open symbols, for a better clarity).

As can be seen from Fig. 8, for $M_*<$ 0.7 $M_\odot$, more massive central stars tend to have faster expanding nebulae. However, part of this apparent correlation is certainly due to selection effects: PN with central stars of small masses - thus evolving slowly - can only be recognized as such when their expansion velocities are not too large, otherwise, they have dispersed in the interstellar medium before the star becomes hot enough to ionize the gas. There is also another factor which comes into the apparent correlation in Fig. 8. This is the fact that the quantities plotted in the figure are not entirely independent. $v_{\rm exp}$ is an observational parameter used in our procedure of determining M_*, and uncertainties in $v_{\rm exp}$ act in the same direction as the correlation seen in Fig. 8. However, we cannot think of any selection effect against PN with small $v_{\rm exp}$ and large M_*.

No $v_{\rm exp}$– M_* correlation is seen for the high mass tail of our sample ($M_*>$ 0.7 $M_\odot$). As seen in Sect. 5, the derived central star masses for these objects are subject to large uncertainties, resulting from our assumption on $M_{\rm neb}$ and/or on observational errors. But in no way do these objects extend the relation observed at $M_*<$ 0.7 $M_\odot$.

The location of point symmetric nebulae in this diagram is remarkable. While the observed correlation between $v_{\rm exp}$ and M_* is rather loose if one considers all the PN morphological types, point symmetric PN present an almost perfect $v_{\rm exp}$ – M_* relation. This correlation would not be destroyed, but simply shifted, if one adopted a different $M_{\rm neb}$ than the value of 0.2 $M_\odot$ used here. This is a further argument that point symmetric PN, compared to other PN morphological classes, form a very specific family.

6.3. The M_* – age diagram

Column 12 of Table 1 lists the PN ages derived from our approach. These are the ages read from the theoretical tracks at the moment when they pass through the positions of the observed objects in our diagrams. Fig. 9 shows these ages as a function of M_*. The meaning of the symbols is the same as in Fig. 8.

This diagram shows that, for objects with $M_*<$ 0.7 $M_\odot$), PN with lower M_* are seen at larger ages than PN with higher M_*. This is expected because high mass central stars evolve more rapidly (see e.g. the predicted variation with time of the nebular Hβ luminosity in Stasińska et al. 1991). If, in addition, PN with higher M_* have faster expanding nebulae (as seen in Fig. 8), then these nebulae will disperse sooner. For $M_*>$ 0.7 $M_\odot$some objects have large ages. But these are precisely the ones having low $v_{\rm exp}$.

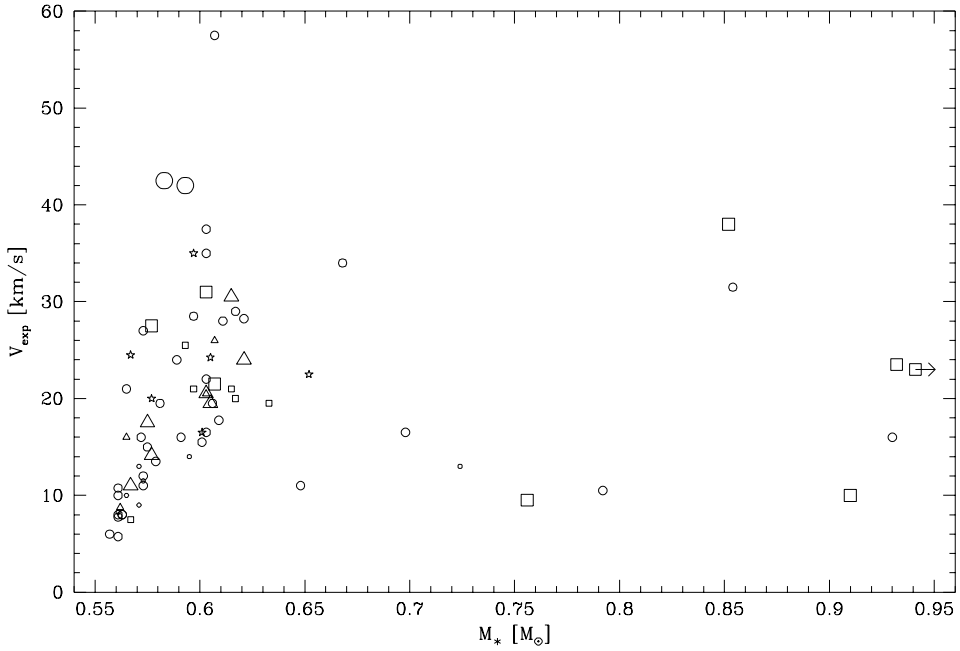

Fig. 8. $v_{\rm exp}$ versus M_* for the different PN morphological types. Elliptical: *e* – small circles, *E* – medium circles, *EH* – large circles; bipolar: *B* – large squares, *BE* – small squares; point symmetric: *P* – large triangles, *PE* – small triangles; d) irregular: *I* – stars.

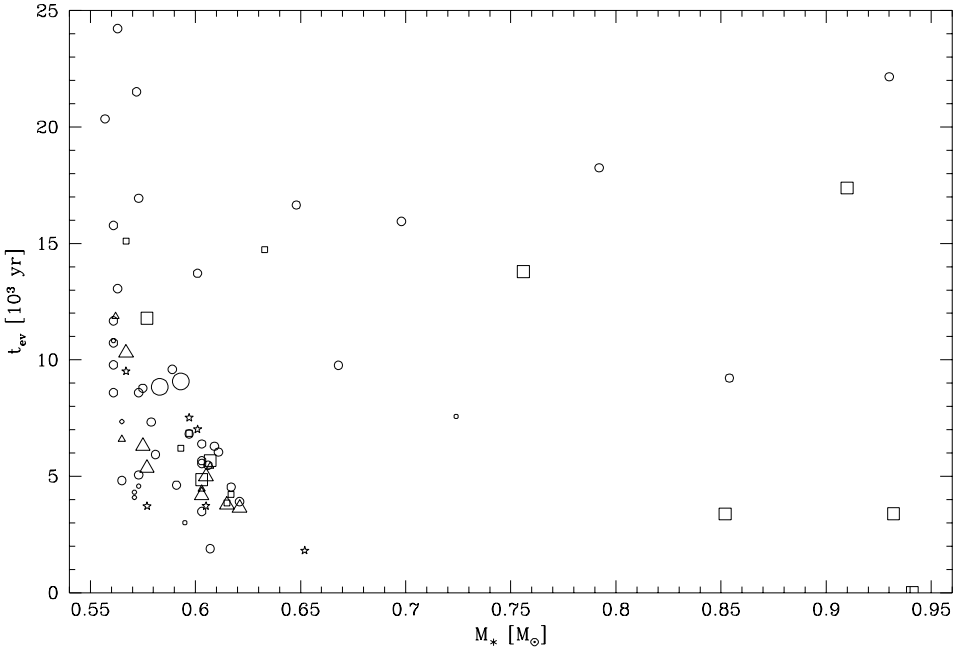

Fig. 9. Evolutionary age versus M_* for different PN morphological types. Same meaning of symbols as in Fig. 8.

When looking at the distribution of PN belonging to different morphological classes, such a diagram could, in principle, tell if any of them corresponds to a transient phenomenon. Indeed, since, during the evolution of a PN, the core mass is unchanged, the fact that a certain morphological type appears only in a narrow time interval could mean that it corresponds to a short evolutionary stage. This seems to be the case for point symmetric nebulae. Such a conclusion would contradict the claim by Amnuel (1995), who finds that PN morphology does not depend on evolution stage. However, the statistics is poor, and definite conclusions cannot be drawn yet. A more populated diagram of this sort is necessary to clear the matter.

6.4. The variation of M_* with Galactic height

The distribution of PN with respect to the Galactic plane is considered to reflect the range of masses of the parent stars. The problem, in such considerations, is to choose a consistent measure of the PN distances. In our approach, along with M_* and age, the model also gives the ratio r of the ionized nebular mass to the assumed total nebular mass. By multiplying the Shklovsky distance by $r^{0.4}$, one then accounts for the overestimation of the distances in the case of optically thick nebulae. There remains, of course, the systematic error due to the choice of $M_{\rm neb}$, but it is only of 30% for a change by a factor two in $M_{\rm neb}$. The distances, d, that we find this way are reported in column 13

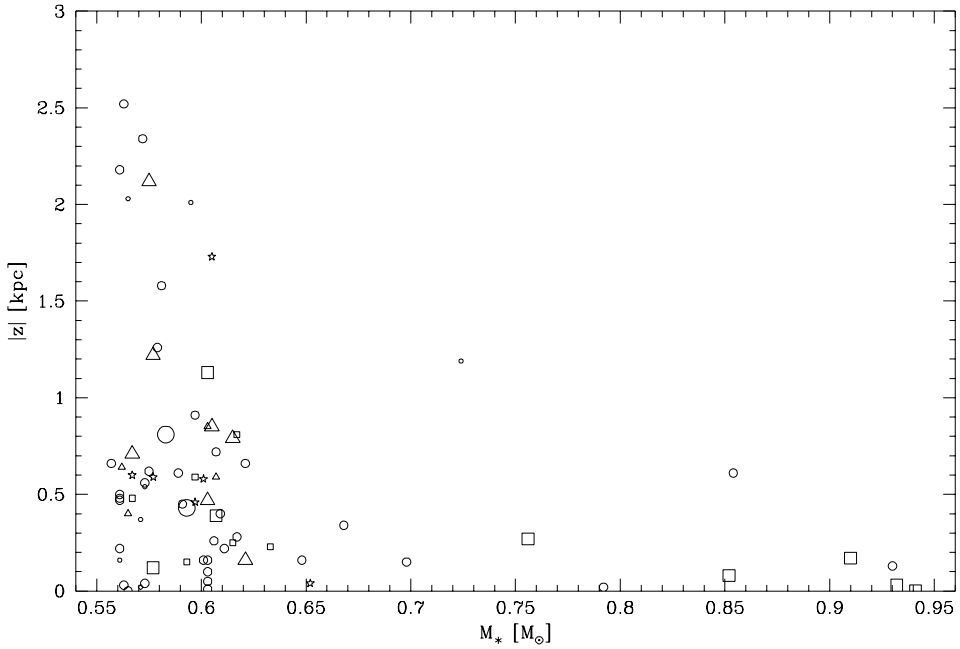

Fig. 10. Distance from the Galactic plane versus M_* for different PN morphological types. Same meaning of symbols as in Fig. 8.

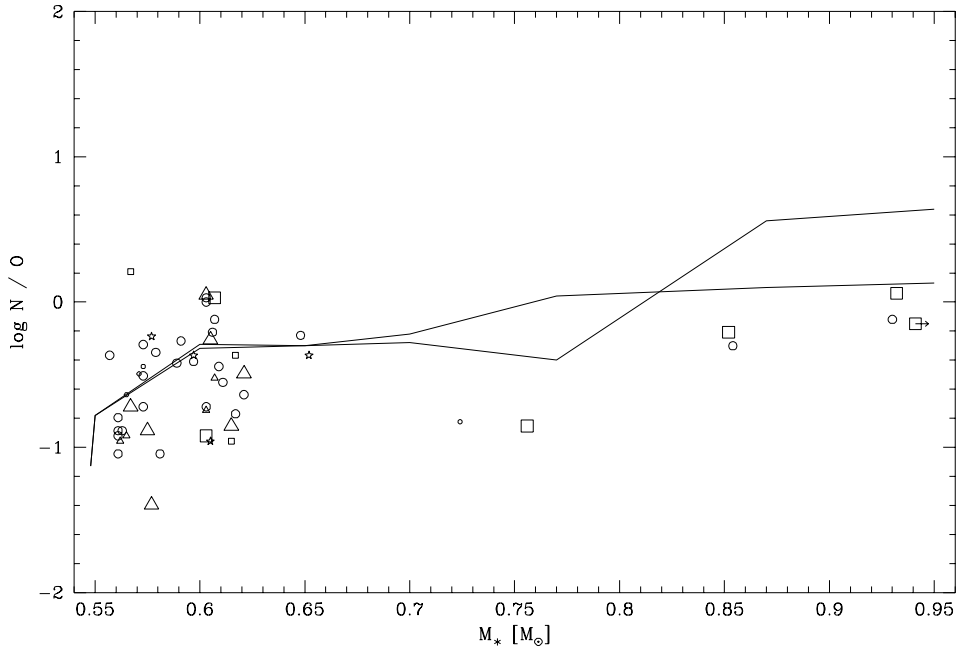

Fig. 11. log N/O versus M_* for different PN morphological types. Same meaning of symbols as in Fig. 8. The two curves represent the prediction from synthetic AGB evolution calculations of Groenewegen et al. (1995) for two different mass loss rate laws.

of Table 1. Note that they are usually close to the Shklovsky distances, because most of the PN are density bounded or not far from it.

Fig. 10 shows how, in our sample, PN with various M_* are distributed as a function of |z|, the distance from the Galactic plane. The meaning of the symbols is the same as in Fig. 8. We see that PN with higher central star masses tend to be found closer to the Galactic plane. This is qualitatively in agreement with the existence of an initial-final mass relation between PN central stars and their progenitors, such as the one found by Weideman (1987).

The mean values of |z| for each of the 4 main morphological classes in our sample are given in Table 2. Similarly to Corradi & Schwarz (1995) we find that bipolar PN seem to be distributed closer to the Galactic plane than the rest of the PN. However, the scale heights we obtain are quite different from theirs. This is due to the fact that our sample is biased against objects at very low Galactic latitude - probably because of our requirement of having good measurements of the stellar magnitudes and expansion velocities - and therefore cannot be used to derive an absolute scale height.

Although the samples are small, it seems that bipolar and point symmetric PN do not have the same vertical distribution

in the Galaxy, indicating that they belong to different stellar populations.

6.5. The relation between M and N/O abundance ratios*

A relation between N/O and central star mass is expected on theoretical grounds if an initial–final mass relation holds, since more massive progenitors dredge up more nitrogen and helium to the surface (Renzini & Voli 1981, Groenewegen et al. 1995). The existence of such a relation has been examined by several authors, with different approaches on the central star mass derivation (e.g. Kaler & Jacoby 1990, Stasińska & Tylenda 1990).

In Fig. 11 are plotted the values of N/O versus our determination of M_*, using the same symbols as in Fig. 8. The N and O abundances have been compiled from recent literature. Table 3[3] lists those data for 100 objects with morphological type assigned by Górny & Stasińska (1995) and not known to have H-poor or binary central stars. Typical errors in N/O are 0.2 dex. Superimposed in Fig. 11 are two curves, representing the predictions from synthetic evolution models for AGB stars by Groenewegen et al. (1995) for two different mass loss rate laws, assuming the Weideman (1987) initial-final mass relation. The general trend predicted by the models is reproduced by the observational points: a rather steep increase log N/O with M_* until about $0.6 M_\odot$, then a much milder increase. However, because of the considerable scatter, a larger sample is required in order to confirm this trend.

Table 2 gives the mean values and dispersions of log N/O for each of the morphological classes (objects for which we could not determine M_* are included in Table 2 as well). We note that the bipolar PN have on average higher N/O ratios than the elliptical ones (as already found by Corradi & Schwarz 1995). The point symmetric PN, on the other hand, tend to have the lowest N/O values. The confidence level of these assertions is 99% using the Mann-Whitney test.

7. Conclusion

The present study has focused on the relation between the PN morphological types and other properties, linked to the central star mass. It has confirmed some of the previous inferences concerning bipolar PN, but on more solid grounds. It has also shown, for the first time, the specific properties of point symmetric PN considered as a class.

The leading idea in our work was that the interpretation of observational parameters of PN central stars, when derived from the observation of the surrounding nebulae, must take into account the biases induced by the techniques used for deriving the stellar parameters. This idea is not new anymore, since the works of Schönberner & Tylenda (1990), Stasińska & Tylenda (1990) or Zhang & Kwok (1993). However, the role played by the expansion velocity has not been fully realized until the work of Górny et al. (1993). We therefore concentrated on a sample of about 80 PN with measured expansion velocities, for which we could assign a morphological type and for which all the parameters necessary for a quantitative analysis were available and sufficiently accurate .

Our approach used a simple evolutionary model for PN, in which the defining parameters are the central star mass, the nebular mass and the expansion velocity. We have proposed a method for deriving the central star parameters (mass, evolution time, distance) where the only unconstrained parameter is the nebular mass (we have studied the effects of changing its value).

We have found a correlation between the nebular expansion velocity and the central star mass, which, however, may be partly due to observational selection effects and may be enhanced by the fact that our derivation of M_* depends on $v_{\rm exp}$. The most remarkable thing about the $M_* - v_{\rm exp}$ diagram is that, while the general scatter is rather large, the point symmetric PN exhibit an almost perfect correlation. This makes them a very specific class of objects.

Point symmetric PN stand out also in other respects. They correspond to a short evolutionary stage. The preliminary analysis in Section 4 suggested that they might be an early phase of the bipolar PN. However, their central stars are, on average, less massive than those of bipolar PN. Also, they are distributed further from the Galactic plane than bipolar PN and tend to have lower N/O. All this indicates that point symmetric PN actually belong to a different population than bipolar PN.

Bipolar PN, compared to the other morphological classes, have the widest distribution of central star masses, with the highest mean value. This is consistent with the fact that, as also found by previous studies, they are on average closer to the Galactic plane, and have higher N/O ratios.

The distribution of PN above the Galactic plane as a function of central star mass is qualitatively consistent with the existence of an initial-final mass relation between PN central stars and their progenitors. Also, the relation we obtain between N/O and M_*, although rather dispersed, looks similar to the one obtained theoretically from evolutionary models for AGB stars.

The follow-up of the present work would be to constitute a larger sample of PN with assigned morphologies and measured basic global parameters ($v_{\rm exp}$, nebular fluxes and angular radii, central star magnitudes) for a more meaningful statistical description of the various classes of PN.

Acknowledgements. S.K. Górny gratefully ackowledges a French grant from the "Projet de co-tutelle de these franco-polonaise" from the French Ministery of Foreign Affairs, and a grant No. 2.P03D.027.10 of the Polish Committee for Scientific Research.

[3] Table 3 is available in electronic form at the CDS

References

Adams S., Seaton M.J., Howarth I.D., Auriere M., Walsh J.R., 1984, MNRAS 207, 417

Amnuel .P, 1995, Ap&SS 225, 275

Balick B., 1987, AJ 94, 671

Barlow M.J., 1987, MNRAS 227, 161

Bässgen M., Bremer M., 1993, in Planetary Nebulae, IAU Symp. 155, R.Weinberger & A.Acker (eds.), Kluwer, p.215

Blöcker T., 1995, A&A 299, 755
Chu Y.H., Jacoby G.H., Arendt R., 1987, ApJS 64, 529
Clegg R.E.S., Peimbert M., Torres-Peimbert S., 1987, MNRAS 224, 761
Corradi R.L.M., Schwarz H.E., 1995, A&A 293, 871
Costa R.D.D., Chiappini C., Maciel W.J., de Freitas Pacheco J.A., 1996, A&AS 116, 1
Costa R.D.D., de Freitas Pacheco J.A., Maciel W.J., 1993, A&A 276, 184
Cuisinier F., Acker A., Köppen J., 1996, A&A 307, 215
Frank A., Balick B., Icke V., Mellema G., 1993, ApJ 404, L25
Frank A., Mellema G, 1994, ApJ 430, 800
Górny S.K., Stasińska G., 1993, A&A. 303, 893
Górny S.K., Tylenda R., Stasińska G., 1993, Acta Astr. 43, 371
Groenewegen M.A.T., van der Hoek L.B., de Jong T., 1995, A&A 293, 381
Kaler J.B., Jacoby G.H., 1990, ApJ 362, 491
Kingsburgh R.L., Barlow M.J., 1994, MNRAS, 271, 257
Livio M. 1994, in Circumstellar Media in the Late Stages of Stellar Evolution, R.E.S.Clegg (ed.), Cambridge University Press, p35
Maciel, W.J., Köppen, J., 1994, A&A 282, 436
Méndez R.H., 1991, in Evolution of Stars: the Photospheric Abundance Connection, IAU Symp. 145, G.Michaud & A.Tutukov (eds.), Reidel, p.375
Peimbert M., Torres-Peimbert S., 1983, in Planetary Nebulae, IAU Symp. 103, D.R.Flower (ed.), Reidel, p.233
Peña M., Ruiz M.T., Maza J., Gonzales L.E., 1989, Rev. Mex. Astrom. Astrofis. 17, 25
Peña M., Ruiz M.T., Torres-Peimbert S., Maza J., 1990, A&A 237, 454
Peña M., Torres-Peimbert S., Peimbert M., Dufour R.J., 1993, Rev. Mex. Astrom. Astrofis. 27, 175
Perinotto M., 1991, ApJ 76, 687
Ratag M., 1991, thesis, University of Groningen
Renzini A., Voli M., 1981, A&A 94, 175
Schönberner D., 1983, ApJ 272, 708
Schönberner D., Tylenda R., 1990, A&A 234, 439
Schwarz H.E., Corradi R.L.M., Melnick J., 1992, A&AS 96, 23
Stanghellini L., Corradi R.L.M., Schwarz H.E., 1993, A&A 279, 521
Stasińska G., Fresneau A., da Silva Gameiro G.F., Acker A., 1991, A&A 252, 762
Stasińska G., Tylenda R., 1990, A&AS 240, 467
Torres-Peimbert S., Peimbert M., 1979, Rev. Mex. Astrom. Astrofis. 4, 341
Tylenda R., 1993, in Planetary Nebulae, IAU Symp. 155, R.Weinberger & A.Acker (eds.), Kluwer, p.423
Tylenda R., Stasińska G., 1994, A&A 284, 897
Tylenda R., Stasińska G., Acker A., Stenholm B., 1991, A&A 246, 221
Walton N.A., Barlow M.J., Clegg R.E.S., 1993, in Planetary Nebulae, IAU Symp. 155, R.Weinberger & A.Acker (eds.), Kluwer, p.581
Weideman V., 1987, A&A 188, 74
Zhang C.Y., 1993, ApJ 410, 239
Zhang C.Y., Kwok S., 1993, ApJS 88, 137

This article was processed by the author using Springer-Verlag LaTeX A&A style file *L-AA* version 3.